Journal of The Electrochemical
Society

Sulfonated Diels-Alder Poly(phenylene) Membrane for Efficient Ion-Selective Transport in Aqueous Metalorganic and Organic Redox Flow Batteries

To cite this article: Brian H. Robb *et al* 2023 *J. Electrochem. Soc.* **170** 030515

Journal of The Electrochemical Society, 2023 **170** 030515
1945-7111/2023/170(3)/030515/9/$40.00 © 2023 The Electrochemical Society ("ECS"). Published on behalf of ECS by IOP Publishing Limited

Sulfonated Diels-Alder Poly(phenylene) Membrane for Efficient Ion-Selective Transport in Aqueous Metalorganic and Organic Redox Flow Batteries

Brian H. Robb,[1,=] Thomas Y. George,[2,=,*] Casey M. Davis,[3,] Zhijiang Tang,[2] Cy H. Fujimoto,[4] Michael J. Aziz,[2,*,z] and Michael P. Marshak[3,5,*,z]**

[1] *Department of Chemical & Biological Engineering, University of Colorado Boulder, Boulder, Colorado, 80303, United States of America*
[2] *John A. Paulson School of Engineering and Applied Sciences, Harvard University, Cambridge, Massachusetts, 02138, United States of America*
[3] *Department of Chemistry, University of Colorado Boulder, Boulder, Colorado, 80303, United States of America*
[4] *Sandia National Laboratories, Nanoscale Sciences Department, Albuquerque, New Mexico, 87185, United States of America*
[5] *Renewable and Sustainable Energy Institute (RASEI), Boulder, Colorado, 80303, United States of America*

Redox flow batteries (RFBs) can achieve long lifetimes and high performance when employing highly selective and conductive membranes. Neutral and alkaline RFBs suffer from higher resistances due to lower cation conductivity, compared to acidic RFBs utilizing proton transport. We report the use of a sulfonated Diels-Alder poly(phenylene) membrane that exhibits low and stable potassium area specific resistance and high efficiency RFB cycling relative to Nafion, as well as undetectable ferricyanide crossover. An alkaline (pH 12) organic anthraquinone derivative RFB using this membrane demonstrates over 10 days of cycling without capacity loss from crossover. A neutral chelated chromium complex RFB using this membrane demonstrates a peak discharge power of $1.23\ \mathrm{W\ cm^{-2}}$, and 80% energy efficiency (EE) cycling at an average discharge power density of $446.3\ \mathrm{mW\ cm^{-2}}$. Finally, the membrane exhibits similar favorable conductivity for many monovalent cations, opening the opportunity to improve the cycling and crossover performance of other acidic, neutral, and alkaline RFBs.
[DOI: 10.1149/1945-7111/acbee6]

Manuscript submitted January 6, 2023; revised manuscript received February 13, 2023. Published March 10, 2023. *This paper is part of the JES Focus Issue on Frontiers of Chemical/Molecular Engineering in Electrochemical Energy Technologies in Honor of Robert Savinell.*

Supplementary material for this article is available online

Renewable energy from intermittent sources such as solar and wind is crucial for decarbonizing electricity generation, but their adoption is limited by the lack of available long duration energy storage.[1] Redox flow batteries (RFBs) constitute a promising platform for providing low cost energy storage, as their all-liquid nature allows for energy and power to be decoupled.[2,3]

RFBs use a membrane or separator to separate the negative electrolyte (negolyte) and positive electrolyte (posolyte). The membrane or separator should permit ionic transport to provide charge balance, while minimizing electroactive species crossover to prevent capacity loss.[4,5] Many RFB chemistries, including all-vanadium, employ metal cations in acid as the electroactive species.[3] These acidic RFBs use proton transport through cation exchange membranes (CEMs) that were adapted from fuel cells, enabling low ohmic resistances.[6,7] However, crossover rates of metal cations through CEMs are high, and addressing this issue is important for the development of these RFB systems.[7–10]

Organic and metalorganic electroactive species represent a promising direction for aqueous RFB electrolyte development.[11–14] Organic reactants with projected decadal lifetime in batteries have been demonstrated, and a strategy of coordinating metal cations with ligands has been successful for enabling high voltage and high concentration aqueous RFBs.[12,15–21] Organic and metalorganic reactants offer drastically lower crossover rates than metal cations due to their increased size and by taking advantage of charge exclusion by, for example, pairing anionic species with CEMs.[5,22,23] However, many of these chemistries Require neutral or alkaline solutions where protons cannot carry the required ionic current. Figure 1a shows a schematic RFB with example aqueous organic and metalorganic electrolytes with potassium carrying charge through a CEM.

The most widely used benchmark CEM is Nafion, a perfluorinated sulfonic acid ionomer (PFSA) which exhibits approximately factor-of-ten lower conductivity of alkali metal cations (e.g., K^+) compared to the protons for which it was designed.[6,24,25] The chemical structure of Nafion contains a Teflon-like perfluorinated backbone with intervals of a flexible side chain tethered to a hydrophilic sulfonic acid moiety (Fig. 1c).[6] Ion conducting channels in Nafion are formed through aggregation of the external sulfonic acid groups in the presence of water. Because the sites for ion exchange, the sulfonate moieties, are tethered to flexible side chains, both the overall water content and the nanostructure of Nafion are dependent on cationic form. Nafion water content decreases with increased cation radius, and larger cations also favor increased aggregation of ionic groups due to rearrangement of the side chains, resulting in more separated water domains.[6,26] These effects amount to an inherent drawback of using Nafion for ion conductivity in alkali metal cation form. Improving membranes for high conductivity of these cations would boost the efficiency and power of neutral and alkaline organic and metalorganic aqueous RFBs.[5]

Recently, membranes based on Diels-Alder poly(phenylene)s (DAPP) have been demonstrated.[27–32] The fluorine containing backbone (FDAPP) has hydrophobic 2,3,4,5,6-pentafluorobenzoyl (PFB) moieties attached onto each pendent aryl ring (6PFB-FDAPP).[27] Depending on the conditions of sulfonation of 6PFB-FDAPP, two different polymers are formed, one with three core aryl rings sulfonated (S-6PFB-FDAPP) and one with all four core aryl rings sulfonated (SS-6PFB-FDAPP). Membranes cast from these polymers are hereafter referred to as **S** and **SS**, respectively. In contrast to the typical PFSA structure, **S** and **SS** have a sulfonated backbone with external hydrophobic moieties (Fig. 1b).[27] These membranes have demonstrated excellent chemical stability in the oxidizing conditions of all-vanadium RFBs, with higher proton conductivity, higher vanadium permeability, and lower selectivity (proton over vanadium

---

[=] Equal Contribution.
[*] Electrochemical Society Member.
[**] Electrochemical Society Student Member.
[z] E-mail: maziz@harvard.edu; michael.marshak@colorado.edu

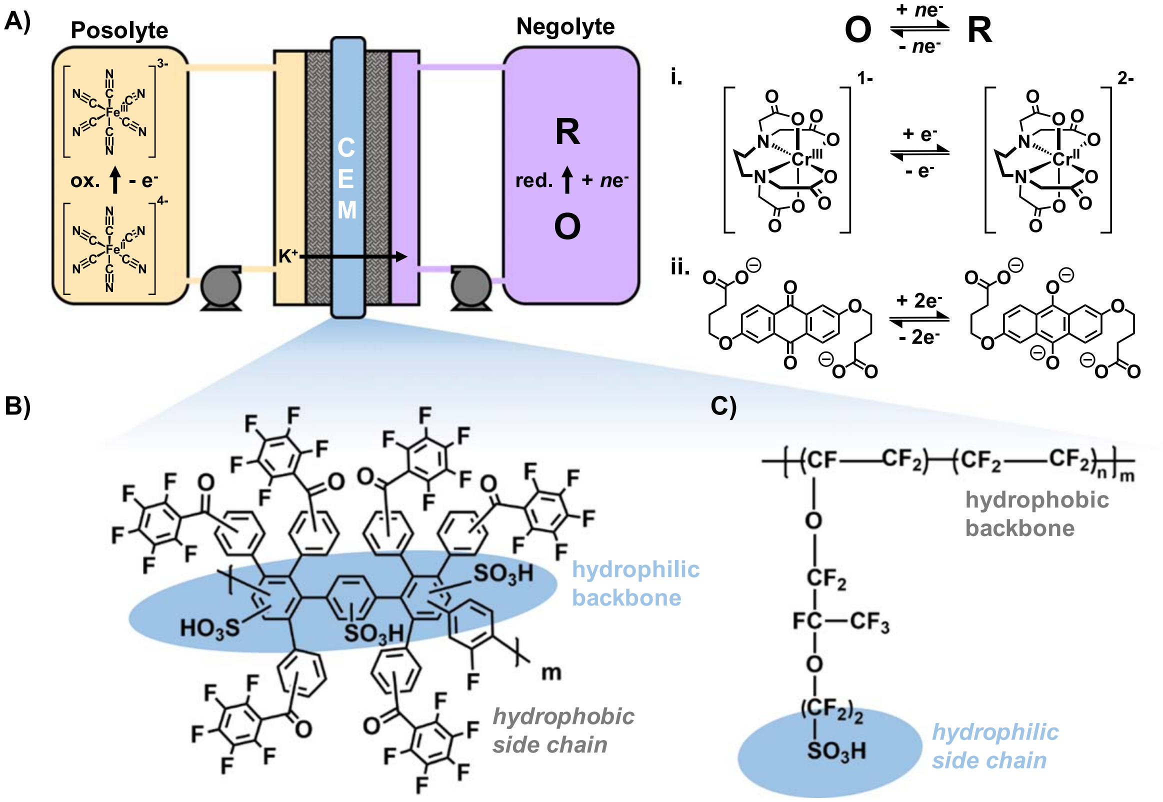

Figure 1. (a) Schematic illustration of a redox flow battery with a posolyte comprising $Fe(CN)_6^{4-/3-}$ and a negolyte chemistry comprising either i. $CrPDTA^{1-/2-}$ or ii. 2–6,$DBEAQ^{2-/4-}$, separated by a CEM conducting potassium ions. The battery is shown in charging mode. CEMs evaluated in this research are (b) a sulfonated Diels Alder poly(phenylene) membrane (**S** is shown, see Fig. S1 for SS structure) and (c) Nafion perfluorinated sulfonic acid ionomer. For both membrane structures, hydrophilic domains are highlighted in blue.

transport) observed for **SS** relative to **S**.[27] However, these 6PFB-FDAPP membranes have been evaluated only in highly acidic conditions. The structure of **S** and **SS** is designed to preclude multiple ion aggregation and to yield narrow, selective hydrophilic domains in aqueous electrolytes. Therefore, this structure is of particular interest for RFBs utilizing alkali metal cations, where it holds promise to improve ion conductivity over Nafion without compromising on selectivity. The present work investigates the impact of this new CEM structure on ionic transport and crossover suppression in aqueous organic and metalorganic RFBs at neutral and alkaline pH, where ionic current is carried by K^+.

As case studies, this research focuses on the prevalent iron(II/III) hexacyanide ($Fe(CN)_6^{4-/3-}$)-based posolyte paired with each of two promising anionic RFB negolytes, comprised of one organic and one metalorganic species, which both use a K^+ counterion and operate at or above pH 7 (Fig. 1a). As an exemplar metalorganic negolyte, we select the highly-reducing (−1.10 V vs SHE) chromium-chelate using the chelating agent 1,3-propylenediaminetetraacetic acid (PDTA) to create the complex $CrPDTA^{1-/2-}$.[33,34] The potassium salt (KCrPDTA) exhibits a high water solubility (1.32 M) and, when paired against $Fe(CN)_6^{4-/3-}$ in an RFB (CrPDTA|$Fe(CN)_6$ RFB) at a pH of 7, a high voltage (1.62 V) and coulombic efficiency (CE) (>99.5%) is observed.[19,33] To represent organic-based negolytes, we select the anthraquinone derivative 4,4’-((9,10-anthraquinone-2,6-diyl)dioxy)dibutyrate (2,6-$DBEAQ^{2-/4-}$, hereafter DBEAQ), which has a demonstrated solubility of up to 0.6 M at pH 12 for the potassium salt (K_2(DBEAQ)), open circuit voltage of 1.05 V paired against $Fe(CN)_6^{4-/3-}$ (DBEAQ|$Fe(CN)_6$ RFB), and extremely stable cycling with a capacity fade rate as low as 0.01%/day.[23] Despite their promising features, each of these chemistries would benefit from improved potassium conductivity in the CEM, without compromising on crossover suppression, to increase voltage efficiency (VE) and prevent capacity fade.

The total area specific resistance (ASR_{tot}) of an RFB, which corresponds to the slope of the polarization curve near current onset (cell voltage vs current density) at a given state of charge, is composed of an ohmic resistance component (ASR_{Ω}) as well as resistances associated with charge transfer and mass transport. ASR_{Ω}, which has contributions from membrane and contact resistances, is generally the largest contributor for organic or metalorganic, non-acidic electrolytes.[24,35] For economic viability, a maximum ASR_{tot} target of 1.5 Ω cm^2 has been proposed for aqueous RFBs.[36,37] Electrochemical impedance spectroscopy (EIS) with 1 M KCl solutions have shown ASR_{Ω} values for RFBs assembled without a membrane, and with H_2O-soaked and 1 M KCl-soaked Nafion NR212 (NR212) membranes to be 0.1 Ω cm^2, 0.8 Ω cm^2, and 2.7 Ω cm^2, respectively, with the H_2O-soaked NR212 resistance increasing over time.[24,38] However, as $Fe(CN)_6^{4-/3-}$ and other organic and metalorganic species have demonstrated crossover through H_2O-soaked NR212, and a prohibitively high resistance is observed with KCl-soaked NR212, there is an opportunity for new membranes to enable efficient, long-duration RFB cycling without crossover.[22,33,39]

Experimental

Materials.—Bismuth chloride oxide (98%) and potassium bromide (99% min) were purchased from Alfa Aesar. Potassium ferricyanide was purchased from LabChem (ACS grade) or from Sigma-Aldrich. Potassium ferrocyanide trihydrate (⩾99%) was purchased from Fluka or from Sigma-Aldrich. Chromium (III) potassium sulfate dodecahydrate (Reagent grade) was purchased from Fisher Science Education. Potassium hydroxide pellets and potassium chloride were purchased from Fisher Chemical (Certified ACS) or from Sigma-Aldrich (reagent grade). 1,3-diaminopropane-N,N,N′,N′-tetraacetic acid (PDTA) (⩾99.0%) was purchased from

Aldrich. 4,4′-((9,10-anthraquinone-2,6-diyl)dioxy)dibutyrate (DBEAQ) was purchased from TCI. These chemicals were used without further purification.

Nafion NR212 (NR212) membranes (nominally 50 μm thick) were purchased from Fuel Cell Store or Ion Power, and Nafion N117 membranes (nominally 183 μm thick) were purchased from Ion Power. Both sulfonated Diels Alder poly(phenylene) membranes with three aryl groups sulfonated (**S**) and all four aryl group sulfonated (**SS**) were prepared at Sandia National Lab and shipped in DI H_2O (to not dry out the already hydrated membranes) for testing. **S** and **SS** membrane thicknesses were measured with a Mitutoyo 547–400 S digital thickness gauge (thicknesses ranging from 15 to 50 um; see Table S1).

All **S** and **SS** membranes were used as received in the H^+ form (H_2O-soaked), or pre-soaked in 1 M KCl (adjusted to pH 12 with KOH for DBEAQ|$Fe(CN)_6$ RFB tests) for at least overnight to ion exchange the membranes from the H^+ form to the K^+ form. Nafion NR212 and N117 were subjected to the same set of pre-treatments as **S** and **SS**, as specified.

Flow cell assembly.—Detailed description of materials and assembly procedures for flow cells used to cycle CrPDTA|$Fe(CN)_6$ RFBs, 2–6,DBEAQ|$Fe(CN)_6$ RFBs, and for EIS measurements with membranes installed in the flow cell hardware with 1 M supporting electrolyte (e.g. 1 M KCl) circulated are provided in Supporting Information (Flow Cell Assembly).

Electrochemical impedance spectroscopy.—All EIS measurements were conducted on a Gamry Interface 5000 potentiostat/galvanostat. All EIS measurements were conducted in triplicate on assembled 5 cm^2 RFBs (assembled as described in Supporting Information—Flow Cell Assembly), and this 5 cm^2 value was used when converting data to area specific resistance. All EIS was performed with the peristaltic pumps turned off.

Time-series and temperature-dependent EIS measurements were performed using a single reservoir of 1 M KCl (100 mL) that was flowed into both sides of the cell. The 100 mL of 1 M KCl was contained in a glass pyrex bottle with a Diba Omnifit 4-hole cap, to minimize H_2O evaporation during the experiment. During elevated temperature EIS, cells were heated for at least 24 hours at each new temperature before EIS was performed to ensure thermal equilibrium of the membrane was reached. EIS in cells with 1 M KCl circulated before and after CrPDTA|$Fe(CN)_6$ RFB operation, and the EIS performed with 1 M MCl solutions (where M is a certain cation, e.g. K^+) circulated, began by flushing DI H_2O (100 mL) followed by 1 M MCl (10 mL) through each side of the RFB. Fresh 1 M MCl (10 mL) was then flowed into both sides of the cell.

MCl EIS data were collected in the frequency range of 5×10^5 Hz to 1×10^4 Hz with 10 data points collected per frequency decade. The DC voltage was 0 V vs the open circuit potential and the AC voltage was 10 mV rms. The RFB was then flushed with 100 mL of DI H_2O through both sides once again, before circulating a new electrolyte. All EIS data was fit using the equivalent circuit model in Fig. S2.

Static diffusion H-cell crossover testing.—Static crossover experiments were performed in custom Adams and Chittenden Scientific Glass Coop H-cells with NW10 Flanges. The receiving reservoir was filled with an osmolarity balanced receiving solution using KCl (12.0 mL of 0.17 M vs KCrPDTA donating electrolyte or 10.0 mL of 0.3 M vs $K_3Fe(CN)_6$ donating electrolyte). The donating electrolyte (0.2 M KCrPDTA or 0.2 M $K_3Fe(CN)_6$) was filled in the other reservoir, such that the volumes and heights of the solutions were equal to prevent a pressure gradient. To determine the amount of KCrPDTA or $K_3Fe(CN)_6$ crossover, UV–vis spectra of aliquots from the receiving solutions were taken periodically without dilution, and then the aliquots were returned to the receiving chamber after measurement.

UV–vis spectrophotometry measurements were performed using an Agilent spectrophotometer using a quartz cuvette with a 1 cm pathlength. The concentration of KCrPDTA solutions was determined using the absorbance at 506 nm (116 M^{-1} cm^{-1}).[40] The concentration of $K_3Fe(CN)_6$ solutions was determined using the absorbance at 420 nm (calibration curve from Fig. S6a). For all samples, the absorbance data was baselined to an absorbance of 0 at 750 nm to account for any drift in the instrument's baseline absorbance that occurred between samples.

Flow battery electrochemical methods.—Detailed procedures for the cycling of CrPDTA|$Fe(CN)_6$ and 2–6,DBEAQ|$Fe(CN)_6$ RFBs, as well as for polarization experiments, are provided in Supporting Information (Flow Battery Electrochemical Methods).

Post-cycling crossover measurements.—Following the conclusion of the room temperature CrPDTA|$Fe(CN)_6$ RFB cycling experiments with **S**, **SS**, and KCl-soaked NR212 membranes, 10 mL of each $Fe(CN)_6^{4-/3-}$ posolyte was fully discharged in an RFB against 10 mL of 0.5 M $K_4Fe(CN)_6$ / 0.1 M $K_3Fe(CN)_6$ electrolyte. This discharge was conducted on a Gamry Interface 1000 potentiostat/galvanostat and consisted of a chronopotentiometric discharge at 100 mA cm^{-2} to a cell potential of −0.4 V, followed by a hold at −0.4 V cell potential for 300 s to ensure full discharge. The discharged post-cycling $Fe(CN)_6^{4-}$ posolyte was then collected for further analysis. The electrolytes from the DBEAQ|$Fe(CN)_6$ RFB tests with **S** and NR212 were also fully discharged (see Supporting Information—Flow Battery Electrochemical Methods) and removed from the glovebox to be subjected to the following analysis.

Cyclic voltammetry (CV) and differential pulse voltammetry (DPV) were conducted using a Gamry Interface 1000 or Gamry Reference 3000 potentiostat/galvanostat, an Ag/AgCl aqueous reference electrode (3 M KCl filling solution) for neutral pH tests or a saturated mercury/mercurous sulfate reference electrode for pH 12, a Pt wire counter electrode, and a 3 mm diameter glassy carbon electrode or an 11 μm diameter carbon fiber ultramicroelectrode as the working electrode. $Fe(CN)_6^{4-}$ solutions that were not already stored in a nitrogen glovebox were first purged with N_2 and then kept under a blanket of argon while tests were performed. For the CrPDTA|$Fe(CN)_6$ RFB chemistry, CVs were conducted at a scan rate of 100 mV s^{-1} and from an initial voltage of −0.5 V vs Ag/AgCl to −1.9 V vs Ag/AgCl and back to −0.5 V vs Ag/AgCl. DPV tests were conducted from an initial voltage of −0.5 V vs Ag/AgCl to a final voltage of −1.7 V vs Ag/AgCl, with a step size of 5 mV, a sample period of 1 s, a pulse time of 0.05 s, and a pulse size of 50 mV. For the DBEAQ|$Fe(CN)_6$ RFB chemistry, CVs were conducted at a scan rate of 10 mV s^{-1} from open circuit between −1 V vs standard hydrogen electrode (SHE) to 1 V vs SHE. DPV tests were conducted over the same range of potentials, with a step size of 5 mV, a sample period of 1 s, a pulse time of 0.05 s, and a pulse size of 50 mV. The carbon fiber ultramicroelectrode was initially pre-treated by holding it at a constant potential of 1.4 V vs SHE for 5 min in 150 mM KCl at pH 9.5 (using KOH), at the start of a new day of experiments.

Results and Discussion

To determine the long-term viability of **S** and **SS** for RFBs utilizing potassium transport, time-based potassium ASR_Ω of H_2O-soaked **S** and **SS** separated RFBs was measured via EIS with 1 M KCl electrolyte. The initial ASR_Ω values for both 6PFB-FDAPP membranes were lower than the 0.8 Ω cm^2 previously seen for H_2O-soaked NR212, and over 7 days, the ASR_Ω for both 6PFB-FDAPP membranes decreased while H_2O-soaked NR212 has been shown to increase (Figs. 2a, S3).[24] To simulate the elevated temperatures that can be achieved in large-scale RFB stacks from resistive heating, temperature-based EIS experiments were then conducted on the 6PFB-FDAPP RFBs and showed a decreasing ASR_Ω with increasing temperature from 20 °C to 50 °C (Fig. S4).[41]

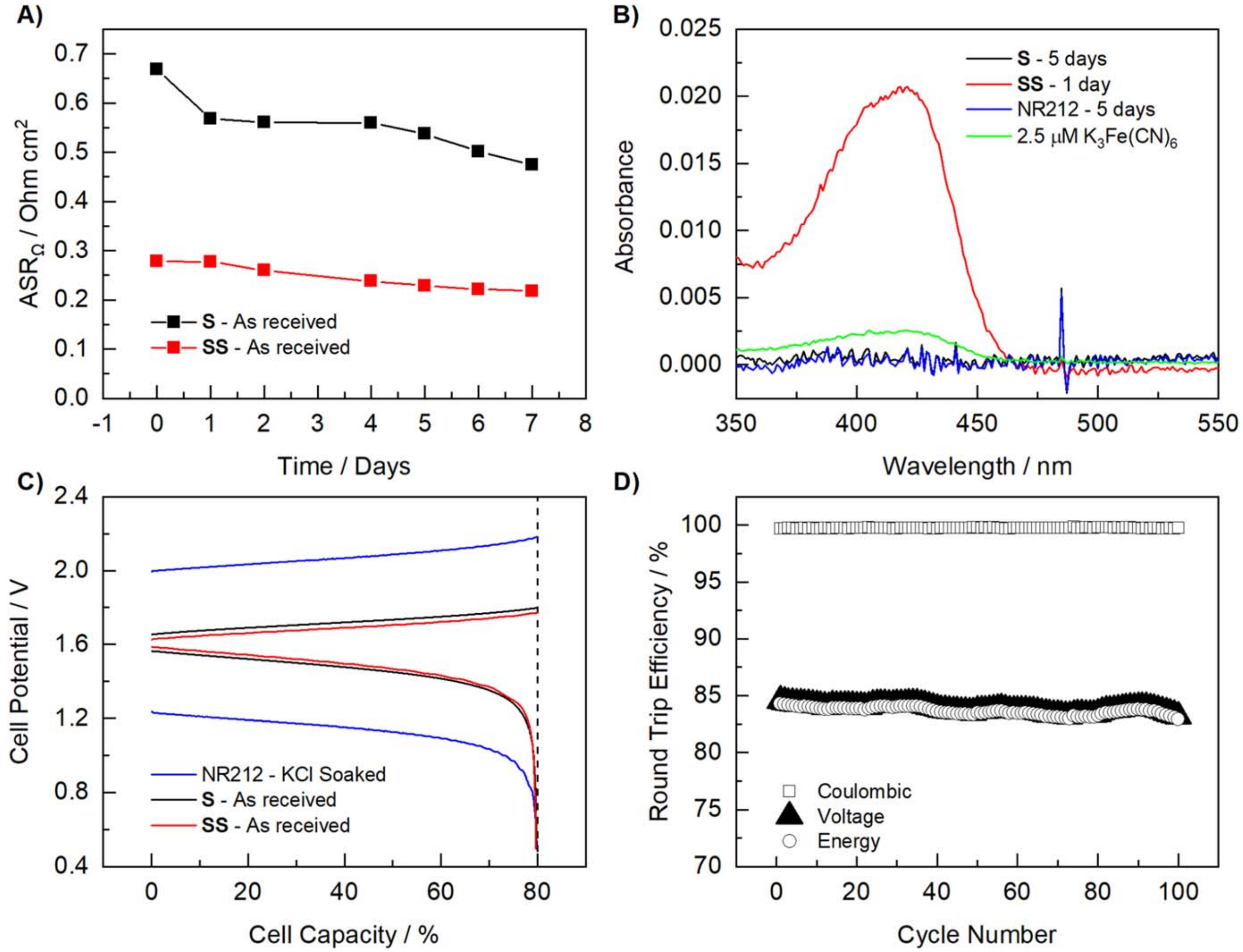

Figure 2. Cell resistance, static crossover UV–vis spectra, and CrPDTA|Fe(CN)$_6$ RFB performance data comparison for select CEMs. (A) Time-based ASR$_\Omega$ of RFBs assembled with as received (H$^+$-form) CEMs, with 1 M KCl solution. (B) UV–vis absorbance spectra of the 0.3 M KCl receiving side of diffusion H-cell experiments for each CEM (K$^+$-form), with 0.2 M K$_3$Fe(CN)$_6$ on the donating side and both electrolytes at pH 12. (C) Cell potential as a function of capacity for a single cycle of 1 M KCrPDTA vs 0.5 M K$_4$Fe(CN)$_6$/0.1 M K$_3$Fe(CN)$_6$ at ±100 mA cm^{-2} with select CEMs. Vertical dashed line represents the 80% capacity of CrPDTA used for cycling. (D) Discharge capacity, CE, VE, and EE vs cycle number for **S** RFB from (C) during 100 cycles at ±100 mA cm^{-2}. All cycles in (D) galvanostatically accessed 80% charging capacity of CrPDTA (0.214 Ah).

These promising conductivities justified static crossover tests of Fe(CN)$_6{}^{3-}$ with both **S** and **SS**.

Static diffusion crossover tests using H-cells were performed to measure the permeation of Fe(CN)$_6{}^{3-}$, the faster-permeating Fe(CN)$_6{}^{4-/3-}$ species, though **S**, **SS**, and NR212, which were pre-soaked in 1 M KCl at pH 12 to ensure complete ion exchange. UV–vis spectrophotometry of an osmolality-balanced 0.3 M KCl receiving solution was used to measure Fe(CN)$_6{}^{3-}$ crossover from a 0.2 M K$_3$Fe(CN)$_6$ donating solution (see Fig. S5 for osmolality measurement). Fe(CN)$_6{}^{3-}$ crossover was observed for **SS**, but crossover though NR212 and **S** was beneath the detection limit of the spectrophotometer (Table I, Fig. 2b). A similar crossover test for KCrPDTA exhibited the same order of magnitude decrease in permeation between the **SS** and the NR212 and **S** membranes (Table S2). Furthermore, as 2,6-DBEAQ has previously demonstrated an order of magnitude lower crossover rate than Fe(CN)$_6{}^{3-}$, the crossover of DBEAQ through NR212 and **S** is expected to be utterly negligible.[15]

To investigate metalorganic cycling performance with the 6PFB-FDAPP membranes, RFBs were assembled with an H$_2$O-soaked **S** (21 μm), H$_2$O-soaked **SS** (22 μm), or KCl-soaked NR212 membrane and utilized a negolyte comprising 10 mL of 1.0 M KCrPDTA with 0.1 M PDTA at pH 7.5 and a posolyte comprising 25 mL of 0.5 M K$_4$Fe(CN)$_6$/0.1 M K$_3$Fe(CN)$_6$ at pH 9.1, a 25% Fe(II) excess. No

Table I. Stirred H-cell crossover results for Fe(CN)$_6{}^{3-}$ through 1 M KCl-soaked membranes.

Membrane	Fe(CN)6^{3}– permeability / cm^2 s^{-1} (test time / days)	Fe(CN)6^{3}– molar flux / μmol cm^{-2} s^{-1}(test time / days)
NR212[a)]	<4 × 10^{-13} (5)	<2 × 10^{-8} (5)
S[a)]	<2 × 10^{-13} (5)	<2 × 10^{-8} (5)
SS	1.2 × 10^{-11} (1)	1.2 × 10^{-6} (1)

a) These values were estimated as upper limits based on a UV–vis detection limit of 1 μM at 420 nm (Fig. S6). The detection limit is not membrane-dependent, but because Nafion NR212 is thicker by a factor of ~2, the permeability upper limit is higher.

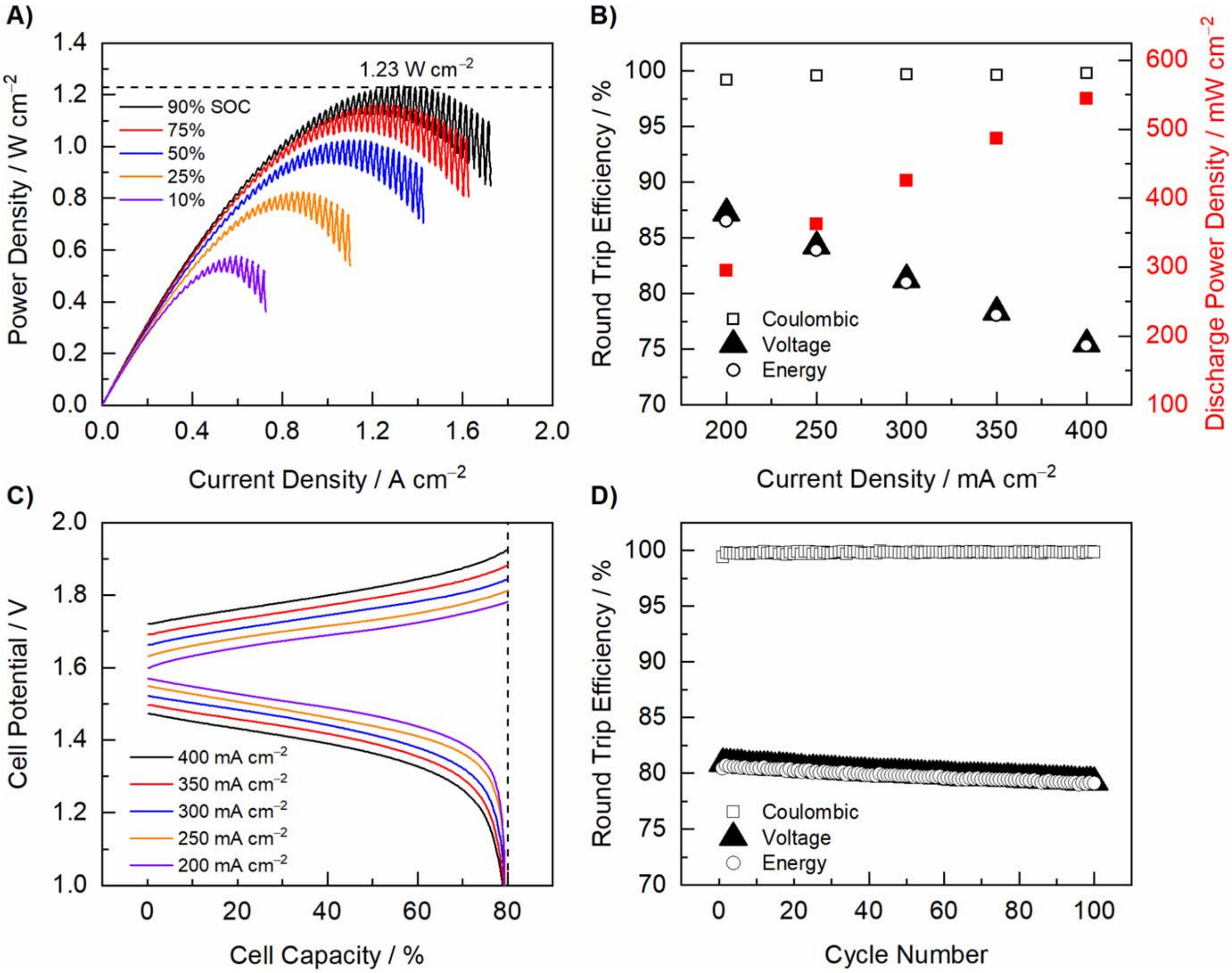

Figure 3. Cell cycling, power, and efficiency data for enhanced **S** RFB utilizing a 12 μm membrane, Bi-plated negolyte electrodes, 40 °C heating, and 1 M KCrPDTA vs 0.5 M $K_4Fe(CN)_6$/0.1 M $K_3Fe(CN)_6$. (A) Discharge power density as a function of current density at select SOC (B) Average efficiencies and discharge power density over 3 cycles at select current densities. (C) Cell potential during a single cycle at select current densities. Vertical dashed line represents the 80% capacity of CrPDTA used for cycling. (D) Discharge capacity, CE, VE, and EE vs cycle number during 100 cycles at ±300 mA cm^{-2}. All cycles in (D) galvanostatically accessed 80% charging capacity of CrPDTA (0.214 Ah).

additional supporting electrolyte was needed in order to have sufficient conductivity for the RFB cycling tests we performed. Prior to cycling, EIS with 1 M KCl was performed to determine initial ASR_Ω (Table II, Figs. S7A, S8A). CrPDTA|Fe(CN)$_6$ RFB cycling with 6PFB-FDAPP membranes consisted of an initial linear current sweep at 500 mA s^{-1} to obtain an ASR_{tot}, followed by linear current sweeps at 500 mA s^{-1} performed at 10, 25, 50, 75, and 90% negolyte state of charge (SOC) to generate polarization and power curves, followed by three cycles to 80% negolyte capacity at select current densities (Figs. 2c, S7–10, Table II). After the galvanostatic cycling, visible crossover of negolyte species into the posolyte was observed with **SS** but not with **S**. The RFB utilizing **S** was then cycled for 100 cycles to 80% negolyte capacity at ±100 mA cm^{-2} with a consistent VE confirmed by an initial and final ASR_{tot} of 1.25 and 1.27 Ω cm^2, respectively, which when combined with the consistent ASR_Ω observed from EIS, indicate that the **S** membrane is stable to the highly reducing CrPDTA conditions (Figs. 2d, S8A, S10). Due to the high ASR_Ω value of the KCl-soaked NR212 RFB, only a linear current sweep to obtain an ASR_{tot} and a single cycle to 80% negolyte capacity at ±100 mA cm^{-2} was performed, with the final charging voltage during this cycle almost reaching 2.2 V (Figs. 2c, S11). The electrolytes in the KCl-soaked NR212 RFB and **SS** RFB were flowed for the same amount of time that the **S** RFB was cycled (4.4 days). A post cycling analysis of each posolyte, using cyclic voltammetry (CV) and differential pulse voltammetry (DPV), confirmed undetectable CrPDTA crossover for the KCl-soaked NR212 and **S** RFBs and the expected CrPDTA crossover for the **SS** RFB (Fig. S12). Therefore, based on both static and RFB-based crossover observations, **S** was selected as the 6PFB-FDAPP membrane to focus on for the remainder of this investigation.

To further enhance the power density enabled by the **S** membrane, cell ASR_{tot} was lowered through the following strategies proven for a CrPDTA|Fe(CN)$_6$ RFB: thinner membrane, elevated temperature operation, and a bismuth electrocatalyst to improve CrPDTA$^{1-/2-}$ redox kinetics.[19,35,38] An RFB was assembled using a 12 μm **S** membrane, cell heating to 40 °C, bismuth-plated negolyte electrodes, and the previously described CrPDTA|Fe(CN)$_6$ RFB electrolytes. This enhanced **S** CrPDTA|Fe(CN)$_6$ RFB demonstrated an initial ASR_{tot} of 0.52 Ω cm^2. Linear current sweeps at 500 mA s^{-1} were performed at 10, 25, 50, 75, and 90% SOC (Figs. 3a, S13). At 90% SOC, between 1.2–1.4 A cm^{-2} an average discharge power density of 1.18 W cm^{-2} was observed, with a peak discharge power density of 1.23 W cm^{-2}, which more than doubles the H_2O-soaked NR212 CrPDTA|Fe(CN)$_6$ RFB reported value of 0.515 W cm^{-2}.[33] Cycling at different current densities was performed, with 3 cycles each at ±200, 250, 300, 350, and 400 mA cm^{-2}

Table II. Cell resistance values, efficiency values at ±100 mA cm^{-2}, peak power density at 90% SOC, and observed CrPDTA$^{1-/2-}$ crossover for S, SS, and NR212 RFBs with 1 M KCl solutions (Initial ASR$_{\Omega}$) or 1.0 M KCrPDTA vs 0.5 M $K_4Fe(CN)_6$/0.1 M $K_3Fe(CN)_6$ (all other columns).

Membrane (Treatment)	Initial ASR$_{\Omega}$ (Ω cm^2)[b,d]	Initial ASR$_{tot}$ (Ω cm^2)	Average CE (%)[e]	Average VE (%)[e]	Peak Power Density at 90% SOC (mW cm^{-2})	CrPDTA Crossover Observed (Y/N)
S (H_2O soaked)	0.69	1.25	99.7	84.4	650	N
SS (H_2O soaked)	0.36	0.86	99.7	86.9	785	Y
NR212 (KCl Soaked)[c]	3.62	4.80	99.8	54.4	N/A	N
NR212(H_2O soaked)[a]	0.84	1.41	99.6	81.1	520	Y

a) Proctor et al. (2022).[35] b) Shorted cell previously demonstrated ASR$_{\Omega}$ of 0.1 Ω cm^2. [24] c) Soaked in 1 M KCl for more than 1 month. d) Conductivity values shown in Table S3. e) **S** and SS are averaged values of 3 cycles with standard deviations <0.1%.

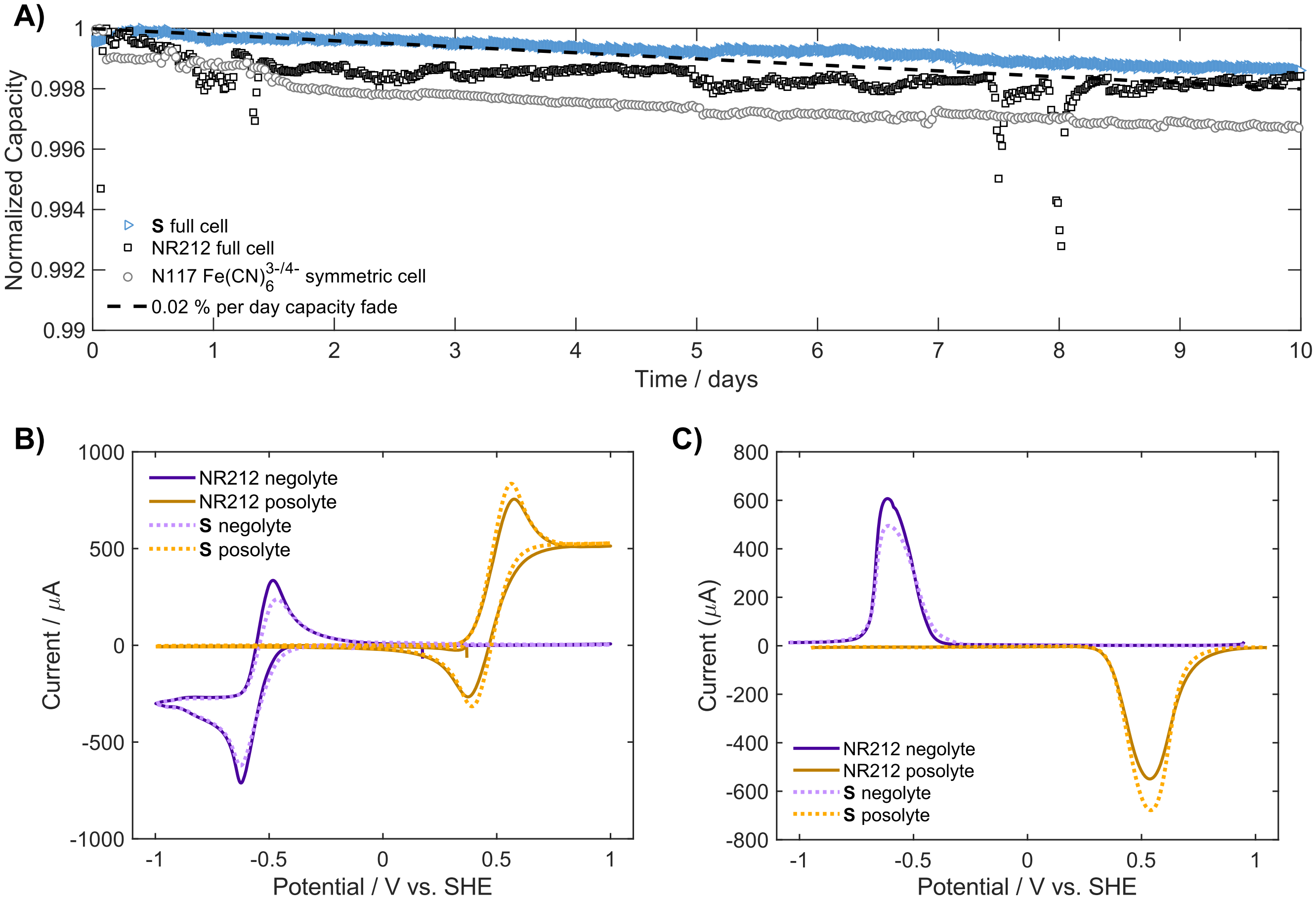

Figure 4. Cell capacity and electrochemical crossover tests for DBEAQ|Fe(CN)$_6$ RFBs with select membrane. (A) Cell capacity over time for 10 days of cell cycling at pH 12 with 8 mL 0.2 M Fe(CN)$_6^{4-/3-}$ as the capacity limiting side. Full cells used 8 mL 0.2 M DBEAQ at pH 12 as the non-capacity limiting side. A volumetrically-unbalanced compositionally-symmetric cell with the same capacity limiting side was devised to minimize concentration gradients for crossover and used 16 mL 0.2 M Fe(CN)$_6^{4-/3-}$ as the non-capacity limiting side, both sides starting at 50% SOC, cycled potentiostatically at ± 0.2 V. (B) Microelectrode cyclic voltammetry of cycled electrolytes from the full cells in (A) does not indicate detectable crossed-over species. (C) Differential pulse voltammetry of cycled electrolytes from the full cells in (A) does not indicate detectable crossed-over species.

to 80% CrPDTA capacity, and greater than 80% energy efficiency (EE) achieved at current densities up to ±300 mA cm^{-2} and average discharge power densities up to 425.5 mW cm^{-2} (Figs. 3b, 3c, S13, Table S4). Linearly interpolating between the 300 and 350 mA cm^{-2} data, an 80% EE could be expected at ±317.1 mA cm^{-2} operation with an expected average discharge power density of 446.3 mW cm^{-2}, which is higher than all but a few optimized all-vanadium RFBs.[42] The cell was then operated for 100 cycles at ±300 mA cm^{-2} and exhibited an average CE of 99.8 ± 0.1% (Figs. 3d, S13, Table S4).

In order to investigate the long term cycling Fe(CN)$_6^{4-/3-}$ crossover performance of **S**, DBEAQ|Fe(CN)$_6$ full cells were assembled using KCl-soaked NR212 or **S** membrane, 8 mL of posolyte comprising 0.2 M K$_3$Fe(CN)$_6$ at pH 12 as the capacity limiting side, and 8 mL of negolyte comprising 0.2 M DBEAQ at pH 12 as the non-capacity limiting side (Supporting Information—Flow Cell Assembly). Similar to the CrPDTA|Fe(CN)$_6$ RFB, no supporting electrolyte was required for cycling, although 0.01 M KOH was provided to adjust the initial pH to 12. Polarization tests showed the RFB with a 25 um thick **S** membrane delivered a peak power density of 119 mW cm^{-2} at 90% SOC, which is more than twice that of the NR212 RFB (Fig. S14). RFBs with the same composition using each membrane were then cycled for approximately 1000 cycles (10 days of cycling with normalized capacity shown in Fig. 4a, extended data in Fig. S15). To access full capacity, galvanostatic cycling at ±100 mA cm^{-2} until a charging voltage cutoff of 1.4 V or a discharging voltage cutoff of 0.6 V was performed followed by a potentiostatic hold at the cutoff until current dropped to ± 2 mA cm^{-2}.

An extremely slow capacity fade rate of 0.01%–0.02% per day for both the **S** and NR212 full cells was observed (Fig. 4a). To assess whether this fade can be attributed to crossover, both electrolytes were completely discharged after cycling and then subjected to cyclic voltammetry (CV) (Figs. 4b and S16) and differential pulse voltammetry (DPV) which both showed no observable crossover of either electroactive species (Fig. 4b). Based on the detection limits of DPV, which was determined to be more sensitive than CV (Figs. S17–18), the crossover flux through **S** during cycling cannot be higher than 9×10^{-8} μmol cm^{-2} s^{-1} for Fe(CN)$_6^{4-/3-}$ (amounting to 0.002%/day) or 2×10^{-7} μmol cm^{-2} s^{-1} for DBEAQ. This means that even the slight capacity fade observed cannot all be crossover. To corroborate this finding, a volumetrically-unbalanced compositionally-symmetric Fe(CN)$_6^{4-/3-}$ cell with the same capacity limiting side as the DBEAQ|Fe(CN)$_6$ RFB and a 16 mL 0.2 M Fe(CN)$_6^{4-/3-}$ non-capacity limiting side (both sides starting at 50% SOC, and cycled potentiostatically at ± 0.2 V) was assembled.[43] In a volumetrically-unbalanced compositionally-symmetric cell, concentration gradients for diffusion across the membrane are diminished to isolate other causes of capacity fade from crossover. The capacity fade rate of this symmetric cell was within standard error of the measured capacity fade rate of the full cells (Table S5), and was in agreement with literature values of Fe(CN)$_6^{4-/3-}$ symmetric cells at pH 12.[44] Therefore, instead of crossover, we attribute the slight capacity fade to the spontaneous

Table III. ASR$_\Omega$ in Ω cm^2 of select RFBs with 1 M MCl solutions at pH 7 except for H$^+$.

Cation	Shorted Cell[a)]	H^+	Li^+	Na^+	K^+	Rb^+	Cs +	NH$_4$+
S[b)]	0.1[a)]	0.18	1.50	0.89	0.56	0.57	0.66	0.52
NR212[a)]	0.1[a)]	0.2	0.8	0.9	2.7	8.1	18.7	1.0

a) Waters et al. (2022) – 1 M MCl soaked NR212 and membraneless cell.[24] b) Conductivity values shown in Table S6.

chemical reduction of ferricyanide to ferrocyanide that has been reported in the literature.[43,44] This mechanism of ferricyanide reduction was observed directly in the symmetric cell in this work using UV–vis spectrophotometry to track the SOC of both capacity limiting and non-capacity limiting sides over the course of cycling (Fig. S19). Thus, we conclude that the **S** membrane allows DBEAQ|Fe(CN)$_6$ RFB cycling that is essentially crossover-free, complementing the results of the **S** membrane Fe(CN)$_6{}^{3-}$ static crossover test.

The **S** membrane has exhibited high performance with undetectable crossover for both metalorganic and organic RFB species. However, while both demonstrated chemistries use potassium ionic transport, some neutral or alkaline chemistries utilize other cations for charge balance. To investigate the applicability of the **S** membrane for chemistries employing other monovalent cations, ASR$_\Omega$ values of an **S** separated RFB were measured via EIS with 1 M HCl, LiCl, NaCl, KCl, RbCl, CsCl, and NH$_4$Cl solutions and compared with equivalent results on NR212 from the literature (Table III, Fig. S20). The **S** membrane resistance values are in the order of the Stokes radius of the ions (e.g. K$^+$ less resistive and Li$^+$ more resistive) which support the hypothesis that the ion conducting channels are not strongly influenced by external electrolyte. This trend is not followed for Nafion, which, conversely, undergoes rearrangement depending on ionic form, and thus exhibits prohibitively high resistance in K$^+$ form. Moreover, for **S** the ASR$_\Omega$ values were below 1.0 Ω cm^2 for all tested cations except Li$^+$, underscoring its promise for a variety of acidic, neutral, and alkaline RFB chemistries.

Conclusions

In this work, two novel cation exchange membranes based on Diels-Alder poly(phenylene) with an external hydrophobic shell and internal hydrophilic core were tested with neutral or alkaline RFB electrolytes that employ potassium membrane transport. Unlike NR212, both as received 6PFB-FDAPP membranes showed improving K$^+$ conductivity over time. Both static and cycling based crossover was undetectable for Fe(CN)$_6{}^{4-/3-}$ with the **S** membrane. The **S** membrane enabled an enhanced CrPDTA|Fe(CN)$_6$ RFB demonstrating an ASR$_{tot}$ of 0.52 Ω cm^2, a peak discharge power of 1.23 W cm^{-2}, and 80% EE cycling at an average discharge power density of 446.3 mW cm^{-2}. Furthermore, long-term cycling crossover elimination was demonstrated with a DBEAQ|Fe(CN)$_6$ RFB over 1000 cycles (>10 days), with no observable crossover of either species and no crossover-based capacity loss. Based on the favorable conductivity of the **S** membrane with a variety of monovalent cations, and the robust chemical stability in oxidative and reducing environments, this membrane shows promise for enabling high performance RFBs with acidic, neutral, or alkaline electroactive species. We attribute the performance of the **S** membrane to its unique structure, enabling a controlled hydrophilic pore and preventing the significant cation-dependent rearrangement exhibited by Nafion. Future work in characterizing the structure of the membrane is warranted in order to better understand the properties that enable its selectivity, and to inform design rules for further high-performance membranes.

Acknowledgments

The information, data, or work presented herein was funded in part by Sandia National Lab subcontract 2290234, and in part by U. S. DOE award DE-AC05–76RL01830 through PNNL subcontract 535264. This material is based upon work supported by the National Science Foundation Graduate Research Fellowship Program under Grant No. DGE 1650115 (supporting B.H.R.) as well as Grant No. DGE 1745303 (supporting T.Y.G.). Any opinions, findings, and conclusions or recommendations expressed in this material are those of the authors and do not necessarily reflect the views of the National Science Foundation. Work at Sandia National Laboratories was supported by the Energy Storage Program, managed by Dr. Imre Gyuk, in the U.S. Department of Energy's Office of Electricity. Sandia National Laboratories is a multi-mission laboratory managed and operated by National Technology & Engineering Solutions of Sandia, LLC, a wholly owned subsidiary of Honeywell International Inc., for the U.S. Department of Energy's National Nuclear Security Administration under contract DE-NA0003525.

Notes

Conflicts of Interest: The University of Colorado has filed a patent on some of the intellectual property disclosed in this manuscript. MPM is the founder of a startup company, Otoro Energy, which is commercializing some of the battery technology reported in this manuscript. MJA is co-founder of, and has a significant ownership stake in, Quino Energy, Inc., which may profit from some of the results reported here.

ORCID

Brian H. Robb https://orcid.org/0000-0002-7181-5720
Thomas Y. George https://orcid.org/0000-0002-0159-8521
Michael J. Aziz https://orcid.org/0000-0001-9657-9456
Michael P. Marshak https://orcid.org/0000-0002-8027-2705

References

1. Annual Energy Outlook, (2019), U.S. Energy Information Administration https://eia.gov/outlooks/aeo/electricity_generation.php (accessed 2019-03-08).
2. Z. Yang, J. Zhang, M. C. W. Kintner-Meyer, X. Lu, D. Choi, J. P. Lemmon, and J. Liu, "Electrochemical energy storage for green grid." *Chem. Rev.*, **111**, 3577 (2011).
3. G. L. Soloveichik, "Flow batteries: current status and trends." *Chem. Rev.*, **115**, 11533 (2015).
4. D. I. Kushner, A. R. Crothers, A. Kusoglu, and A. Z. Weber, "Transport phenomena in flow battery ion-conducting membranes." *Curr. Opin. Electrochem.*, **21**, 132 (2020).
5. C. A. Machado, G. O. Brown, R. Yang, T. E. Hopkins, J. G. Pribyl, and T. H. Epps, "Redox flow battery membranes: improving battery performance by leveraging structure–property relationships." *ACS Energy Lett.*, **6**, 158 (2021).
6. A. Kusoglu and A. Z. Weber, "New insights into perfluorinated sulfonic-acid ionomers." *Chem. Rev.*, **117**, 987 (2017).
7. B. G. Thiam and S. Vaudreuil, "Review—recent membranes for vanadium redox flow batteries." *J. Electrochem. Soc.*, **168**, 070553 (2021).
8. D. Düerkop, H. Widdecke, C. Schilde, U. Kunz, and A. Schmiemann, "Polymer membranes for all-vanadium redox flow batteries: a review." *Membranes*, **11**, 214 (2021).
9. R. Darling, K. Gallagher, W. Xie, L. Su, and F. Brushett, "Transport property requirements for flow battery separators." *J. Electrochem. Soc.*, **163**, A5029 (2016).
10. M. L. Perry, J. D. Saraidaridis, and R. M. Darling, "Crossover mitigation strategies for redox-flow batteries." *Curr. Opin. Electrochem.*, **21**, 311 (2020).
11. R. Darling, "Techno-economic analyses of several redox flow batteries using levelized cost of energy storage." *Curr. Opin. Chem. Eng.*, **37**, 1 (2022).
12. J. R. Thurston, S. E. Waters, B. H. Robb, M. P. Marshak, and L. F. Cabeza, "Organic and metal-organic RFBs." *Encyclopedia of Energy Storage* (Amsterdam) (Elsevier) Vol. 2, p. 423 (2022).
13. B. Huskinson, M. P. Marshak, C. Suh, S. Er, M. R. Gerhardt, C. J. Galvin, X. Chen, A. Aspuru-Guzik, R. G. Gordon, and M. J. Aziz, "A metal-free organic–inorganic aqueous flow battery." *Nature*, **505**, 195 (2014).
14. K. Lin et al., "Alkaline quinone flow battery." *Science*, **349**, 1529 (2015).

15. D. G. Kwabi, Y. Ji, and M. J. Aziz, "Electrolyte lifetime in aqueous organic redox flow batteries: a critical review." *Chem. Rev.*, **120**, 6467 (2020).
16. Y. Ji, M.-A. Goulet, D. A. Pollack, D. G. Kwabi, S. Jin, D. D. Porcellinis, E. F. Kerr, R. G. Gordon, and M. J. Aziz, "A phosphonate-functionalized quinone redox flow battery at near-neutral ph with record capacity retention rate." *Adv. Energy Mater.*, **9**, 1900039 (2019).
17. M. Wu, Y. Jing, A. A. Wong, E. M. Fell, S. Jin, Z. Tang, R. G. Gordon, and M. J. Aziz, "Extremely stable anthraquinone negolytes synthesized from common precursors." *Chem*, **6**, 1432 (2020).
18. Y. Jing et al., "Anthraquinone flow battery reactants with nonhydrolyzable water-solubilizing chains introduced via a generic cross-coupling method." *ACS Energy Lett.*, **7**, 226 (2022).
19. B. H. Robb, S. E. Waters, and M. P. Marshak, "High energy density chelated chromium flow battery electrolyte at neutral PH." *Chem. - Asian J.*, **17**, e202200700 (2022).
20. D. Reber, J. R. Thurston, M. Becker, G. F. Pach, M. E. Wagoner, B. H. Robb, S. E. Waters, and M. P. Marshak, "Mediating anion-cation interactions to improve aqueous flow battery electrolytes." *Appl. Mater. Today*, **28**, 101512 (2022).
21. B. H. Robb, S. E. Waters, and M. P. Marshak, "Evaluating aqueous flow battery electrolytes: a coordinated approach." *Dalton Trans.*, **49**, 16047 (2020).
22. C. Noh, M. Shin, and Y. Kwon, "A strategy for lowering cross-contamination of aqueous redox flow batteries using metal-ligand complexes as redox couple." *J. Power Sources*, **520**, 230810 (2022).
23. D. G. Kwabi et al., "Alkaline quinone flow battery with long lifetime at PH 12." *Joule*, **2**, 1894 (2018).
24. S. E. Waters, J. R. Thurston, R. W. Armstrong, B. H. Robb, M. P. Marshak, and D. Reber, "Holistic design principles for flow batteries: cation dependent membrane resistance and active species solubility." *J. Power Sources*, **520**, 230877 (2022).
25. A. Z. Weber, M. M. Mench, J. P. Meyers, P. N. Ross, J. T. Gostick, and Q. Liu, "Redox flow batteries: a review." *J. Appl. Electrochem.*, **41**, 1137 (2011).
26. W. Y. Hsu and T. D. Gierke, "Ion transport and clustering in nafion perfluorinated membranes." *J. Membr. Sci.*, **13**, 307 (1983).
27. S. Maurya, E. Baca, K. K. Bejagam, H. Pratt, T. Anderson, R. Mukundan, and C. Fujimoto, "Durable and highly selective ion transport of a sulfonated diels alder poly (phenylene) for vanadium redox flow batteries." *J. Power Sources*, **520**, 230805 (2022).
28. C.-N. Sun, Z. Tang, C. Belcher, T. A. Zawodzinski, and C. Fujimoto, "Evaluation of diels–alder poly(phenylene) anion exchange membranes in all-vanadium redox flow batteries." *Electrochem. Commun.*, **43**, 63 (2014).
29. C. Fujimoto, S. Kim, R. Stains, X. Wei, L. Li, and Z. G. Yang, "Vanadium redox flow battery efficiency and durability studies of sulfonated diels alder poly (phenylene)s." *Electrochem. Commun.*, **20**, 48 (2012).
30. E. J. Park, S. Maurya, M. R. Hibbs, C. H. Fujimoto, K.-D. Kreuer, and Y. S. Kim, "Alkaline stability of quaternized diels–alder polyphenylenes." *Macromolecules*, **52**, 5419 (2019).
31. Z. Tang, J. S. Lawton, C.-N. Sun, J. Chen, M. I. Bright, A. M. Jones, A. B. Papandrew, C. H. Fujimoto, and T. A. Zawodzinski, "Characterization of sulfonated diels-alder poly(phenylene) membranes for electrolyte separators in vanadium redox flow batteries." *J. Electrochem. Soc.*, **161**, A1860 (2014).
32. A. M. Pezeshki, Z. J. Tang, C. Fujimoto, C.-N. Sun, M. M. Mench, and T. A. Zawodzinski, "Full cell study of diels alder poly(phenylene) anion and cation exchange membranes in vanadium redox flow batteries." *J. Electrochem. Soc.*, **163**, A5154 (2016).
33. B. H. Robb, J. M. Farrell, and M. P. Marshak, "Chelated chromium electrolyte enabling high-voltage aqueous flow batteries." *Joule*, **3**, 2503 (2019).
34. H. Ogino, T. Nagata, and K. Ogino, "Redox potentials and related thermodynamic parameters of (diaminopolycarboxylato)metal(iii/ii) redox couples." *Inorg. Chem.*, **28**, 3656 (1989).
35. A. D. Proctor, B. H. Robb, J. D. Saraidaridis, and M. P. Marshak, "Bismuth electrocatalyst enabling reversible redox kinetics of a chelated chromium flow battery anolyte." *J. Electrochem. Soc.*, **169**, 030506 (2022).
36. R. Dmello, J. D. Milshtein, F. R. Brushett, and K. C. Smith, "Cost-driven materials selection criteria for redox flow battery electrolytes." *J. Power Sources*, **330**, 261 (2016).
37. R. M. Darling, K. G. Gallagher, J. A. Kowalski, S. Ha, and F. R. Brushett, "Pathways to low-cost electrochemical energy storage: a comparison of aqueous and nonaqueous flow batteries." *Energy Environ. Sci.*, **7**, 3459 (2014).
38. B. H. Robb, S. E. Waters, J. D. Saraidaridis, and M. P. Marshak, "Realized potential as neutral ph flow batteries achieve high power densities." *Cell Rep. Phys. Sci.*, **3**, 101118 (2022).
39. J. D. Saraidaridis, R. M. Darling, Z. Yang, M. E. Fortin, C. Shovlin, B. H. Robb, S. E. Waters, and M. P. Marshak, "Transport of Ligand Coordinated Iron and Chromium through Cation-Exchange Membranes." *J. Electrochem. Soc.*, **169**, 060532 (2022).
40. M. Hecht, F. A. Schultz, and B. Speiser, "Ligand structural effects on the electrochemistry of chromium(iii) amino carboxylate complexes." *Inorg. Chem.*, **35**, 5555 (1996).
41. L. Li et al., "A stable vanadium redox-flow battery with high energy density for large-scale energy storage." *Adv. Energy Mater.*, **1**, 394 (2011).
42. H. R. Jiang, J. Sun, L. Wei, M. C. Wu, W. Shyy, and T. S. Zhao, "A high power density and long cycle life vanadium redox flow battery." *Energy Storage Mater.*, **24**, 529 (2020).
43. M.-A. Goulet and M. J. Aziz, "Flow battery molecular reactant stability determined by symmetric cell cycling methods." *J. Electrochem. Soc.*, **165**, A1466 (2018).
44. E. Fell, D. D. Porcellinis, Y. Jing, V. Gutierrez-Venegas, R. Gordon, S. Granados-Focil, and M. Aziz, *ChemRxiv* (2022), Long-term stability of ferri-/ferrocyanide as an electroactive component for redox flow battery applications: on the origin of apparent capacity fade 10.26434/chemrxiv-2022-zl7l6.